A Splicing Variant in *XPA* Results in Delayed Onset of Clinical Features of Xeroderma Pigmentosum

Anita van den Heuvel[1], Annelotte P. Wondergem[1], Mihyun Kim[2,3], Isa Breet[1], Hyun Suk Kim[2], Heather Fawcett[4], Hiva Fassihi[5], Alan R. Lehmann[4,5], Orlando D. Schärer[2,3,6] and Martijn S. Luijsterburg[1]

Journal of Investigative Dermatology (2025) ■, ■–■; doi:10.1016/j.jid.2025.08.047

Xeroderma pigmentosum (XP) is a rare autosomal recessive disorder characterized by defective nucleotide excision repair (NER), leading to extreme sensitivity to sunlight-induced skin pigmentation changes and increased skin cancer risk. Patients with XP present with varying severity, often influenced by specific variants in NER-associated genes. In this study, we describe 2 unrelated Cypriot patients with XP-A with a mild phenotype linked to a homozygous missense variant in *XPA* (ENST00000375128.5:c.389G>A/ENSP00000364270.5:p.R130K, further referred to as $XPA^{c.389G>A}$/XPA^{R130K}). The older patient, aged 69 years, developed progressive neurological degeneration in his 40s, whereas the younger patient, aged 32 years, has no neurological abnormalities to date. Molecular analysis revealed a severe transcription-coupled NER defect and reduced global genome repair (global genome NER) in patient fibroblasts, consistent with the XP-A diagnosis. Surprisingly, very low XPA protein levels were detected, despite the conservative amino acid substitution. Further experiments demonstrated that although the XPA^{R130K} protein variant is both stable and functional in NER, it is a splice defect in the $XPA^{c.389G>A}$ gene in patients that leads to reduced *XPA* mRNA levels, ultimately explaining the low protein levels and residual NER activity in patients. This study highlights the complex relationship between genotype, splicing, and clinical phenotype in patients with XP-A.

Keywords: DNA repair, Nucleotide excision repair, Splicing, Xeroderma pigmentosum, XPA

INTRODUCTION

Nucleotide excision repair (NER) is a pathway responsible for removing DNA damage caused by UV light from the sun or by chemical carcinogens that produce bulky DNA lesions (Kraemer et al, 2007; Lehmann, 2003). Xeroderma pigmentosum (XP) is a rare autosomal recessive disorder characterized by extreme sensitivity to sunlight, leading to pigmentation changes and a markedly increased risk of developing skin cancers. Approximately 50% of patients exhibit acute sunburn sensitivity, and about 30% develop progressive neurological abnormalities that often result in early death. Patients with XP have been assigned to 7 genetic complementation groups (XP-A–XP-G), whose corresponding genes encode proteins involved in NER, and an eighth so-called variant group (XP-V), whose gene encodes DNA polymerase eta, which is involved in DNA synthesis past UV lesions.

NER consists of several steps, including the recognition of DNA damage, unwinding of the DNA around the lesion, and dual incision on both sides of the damage. This is followed by filling in the resulting gap and ligating the newly synthesized DNA to the existing strand (Evans et al, 1997; Missura et al, 2001; Riedl et al, 2003; Volker et al, 2001). The mechanism of damage recognition depends on the location of the lesion. On the transcribed strand of actively transcribed DNA, damage stalls RNA polymerase II, triggering transcription-coupled NER (TC-NER). This pathway is initiated by the CSA and CSB proteins, which are defective in Cockayne syndrome, as well as by UVSSA, which is defective in UV-sensitive syndrome (Nakazawa et al, 2020, 2012; van den Heuvel et al, 2021; van der Weegen et al, 2020). In the rest of the genome, damage is recognized by the DDB2 and XPC proteins, which are specific to global genome NER (GG-NER) (Itoh, 2006; Luijsterburg et al, 2012, 2007; Moser et al, 2005; Rapić-Otrin et al, 2003; Sugasawa and Hanaoka, 2007; Sugasawa et al, 1998). The 2 pathways then converge with the recruitment of the repair-transcription factor TFIIH.

[1]*Department of Human Genetics, Leiden University Medical Center, Leiden, The Netherlands;* [2]*Center for Genomic Integrity, Institute for Basic Science, Ulsan, Republic of Korea;* [3]*Department of Biological Sciences, Ulsan National Institute of Science and Technology, Ulsan, Republic of Korea;* [4]*Genome Damage and Stability Centre, University of Sussex, Brighton and Hove, United Kingdom;* [5]*National Xeroderma Pigmentosum Service, Guy's and St Thomas' Foundation Trust, London, United Kingdom; and* [6]*UPMC Hillman Cancer Center, Department of Pharmacology and Chemical Biology, University of Pittsburgh School of Medicine, Pittsburgh, Pennsylvania, USA*

Correspondence: Martijn Luijsterburg, Department of Human Genetics, Leiden University Medical Center (LUMC), Einthovenweg 20, Leiden 2333 ZC, Netherlands. E-mail: m.luijsterburg@lumc.nl

Abbreviations: EdU, 5-ethynyl-deoxy-uridine; EU, 5-ethynyl-uridine; FCS, fetal calf serum; GG-NER, global genome nucleotide excision repair; NER, nucleotide excision repair; RRS, recovery of RNA synthesis; TC-NER, transcription-coupled nucleotide excision repair; UDS, unscheduled DNA synthesis; XP, xeroderma pigmentosum

Received 11 April 2025; revised 29 August 2025; accepted 29 August 2025; accepted manuscript published online XXX; corrected proof published online XXX

The second protein to join the general NER complex is XPA, a small scaffold protein of 273 amino acids, encoded on 6 exons, which has binding sites for DNA and for several of the other proteins involved in NER (Sugitani et al, 2016). As such, it coordinates the assembly of the NER proteins in the correct configuration (Kim et al, 2022). Truncating variants causing complete loss of XPA protein result in very severe cutaneous and neurological features (Satokata et al, 1992a, 1992b). However, residual XPA function can lead to milder clinical features. Truncations close to the C-terminus, resulting in reduced interaction with TFIIH, delay the onset of neurological problems (Kobayashi et al, 1998; Nishigori et al, 1993; Takahashi et al, 2010; Weerd-Kastelein et al, 1976). A pathogenic variant found in populations from North India and Pakistan (ENST00000375128.5:c.555+8A>G) generates a new splice site in intron 4 and causes a drastic reduction in NER activity. However, 5% of the mRNA is correctly spliced, giving rise to approximately 5% residual protein, which is sufficient to abolish neurological problems and reduce the sensitivity of the skin to pigmentation changes and skin cancers (Sethi et al, 2016). A missense variant resulting in the substitution p.H244R (ENSP00000364270.5:p.H244R) was found recently in 2 patients with mild cutaneous features but marked neurological abnormalities. Although GG-NER was reduced to just 50% of normal, TC-NER activity was nearly undetectable in cells from these patients (van den Heuvel et al, 2023).

In this study, we report on 2 unrelated Cypriot patients with a homozygous missense variant in *XPA* (ENST00000375128.5:c.389G>A, ENSP00000364270.5:p.R130K, further referred to as $XPA^{c.389G>A}$ or XPA^{R130K}, respectively) associated with abnormal splicing. The older patient had no neurological problems until his 40s, since when he has shown progressive neurological degeneration. The younger patient has, to date, exhibited no neurological problems.

RESULTS

Two unrelated Cypriot patients with mild XP-A

The older patient (XP134BR) is aged 69 years (Supplementary Figure S1a). His parents were from Cyprus, but he was born and raised in the United Kingdom. He was diagnosed with XP-A at the age of 65 years. He had been a successful businessman, but in his mid-40s, he started to develop neurological problems: initially, cerebellar ataxia resulting in frequent falls and 2 road traffic accidents. Hearing impairment was noted in his early 40s and he has worn hearing aids since the age of 49 years. Audiometry demonstrates profound sensorineural hearing loss. He is now severely dysarthric with significant cognitive impairment. He has difficulties in swallowing with recurrent choking episodes. He is non-ambulatory with absent reflexes throughout and is unable to carry out activities of daily living. Magnetic resonance imaging brain scan shows cerebellar atrophy and a frontal meningioma. He has had progressive exposed-site lentigines from the age of 3 years and has always had easy and prolonged sunburn reactions, lasting up to 2 weeks. He has had many sunny holidays abroad but generally stays out of the sun. He has had approximately 8 in situ melanomas and melanoma skin cancers from the age of 59 years, all on his head and neck. He has 4 children, and there is no other family history of XP. He continues to deteriorate neurologically.

The unrelated younger patient (XP133BR) is aged 32 years (Supplementary Figure S1a). She works as an office administrator in Cyprus and was diagnosed with XP-A at the age of 28 years. She has had progressive exposed-site lentigines from the age of 2 years and reports exaggerated sunburn reactions during the summer months in Cyprus, occurring within about 10 minutes of sun exposure, which can take up to 5 days to resolve. She has had 4 melanoma skin cancers, on the arms and legs, the first at the age of 28 years. She is now very careful with sun protection. On direct questioning, she does not report any problems with balance, hearing, or memory. Clinically, she does not demonstrate any overt neurological findings, and her audiometry and nerve conduction studies are normal, but a recent magnetic resonance imaging brain scan has shown global cerebellar atrophy. She will be monitored closely for new neurological abnormalities. There is no other family history of XP.

Molecular analysis

Molecular analysis revealed that both patients were homozygous for the *XPA* variant c.389G>A. At the protein level, this variant is expected to result in the conservative amino acid substitution p.R130K, which is unlikely to account for the mild XP-A phenotype observed in these patients. XPA engages with the NER complex once TFIIH begins to open the DNA duplex around the lesion. XPA binds at the single-stranded/double stranded DNA junction 5′ to the lesion, where it first facilitates lesion verification by TFIIH (Kim et al, 2023; Kokic et al, 2019). It then stabilizes the open complex and serves as a scaffold for the binding of RPA and ERCC1 to the preincision complex. The XPA^{R130} residue makes contact with the single-stranded DNA, near the binding site of RPA70 (Topolska-Woś et al, 2020) (Supplementary Figure S1b). Although XPA^{R130} likely contributes to DNA binding, our previous work has shown that multiple mutations are required to disrupt the XPA–DNA and XPA–RPA interfaces (Kim et al, 2022), suggesting that a single conservative amino acid change would have a minimal effect. Nevertheless, to further investigate this, we decided to measure the NER capacity in patient-derived fibroblasts.

Defective transcription recovery after UV irradiation in patient cells

Fibroblast cell cultures were established from both patients, designated XP133BR and XP134BR. To measure TC-NER, we visualized nascent transcription by 5-ethynyl-uridine (EU) labeling after global UV irradiation in primary fibroblasts. After UV irradiation, transcribing RNA polymerase II stalls at the lesion, resulting in significantly reduced transcription levels. The recovery of RNA synthesis (RRS) after UV irradiation is fully dependent on the activity of TC-NER (Mayne and Lehmann, 1982). Wild-type 48BR primary fibroblasts recovered from the UV-induced transcription arrest within 24 hours after UV irradiation, whereas no recovery could be detected in either XP133BR or XP134BR cells (Figure 1a and b). In fact, transcription recovery was as low as detected in primary fibroblasts from a patient with severe XP-A (XP15BR [Fassihi et al, 2016]) with a frameshift variant (ENSP00000364270.5:p.V90fs), which were included in

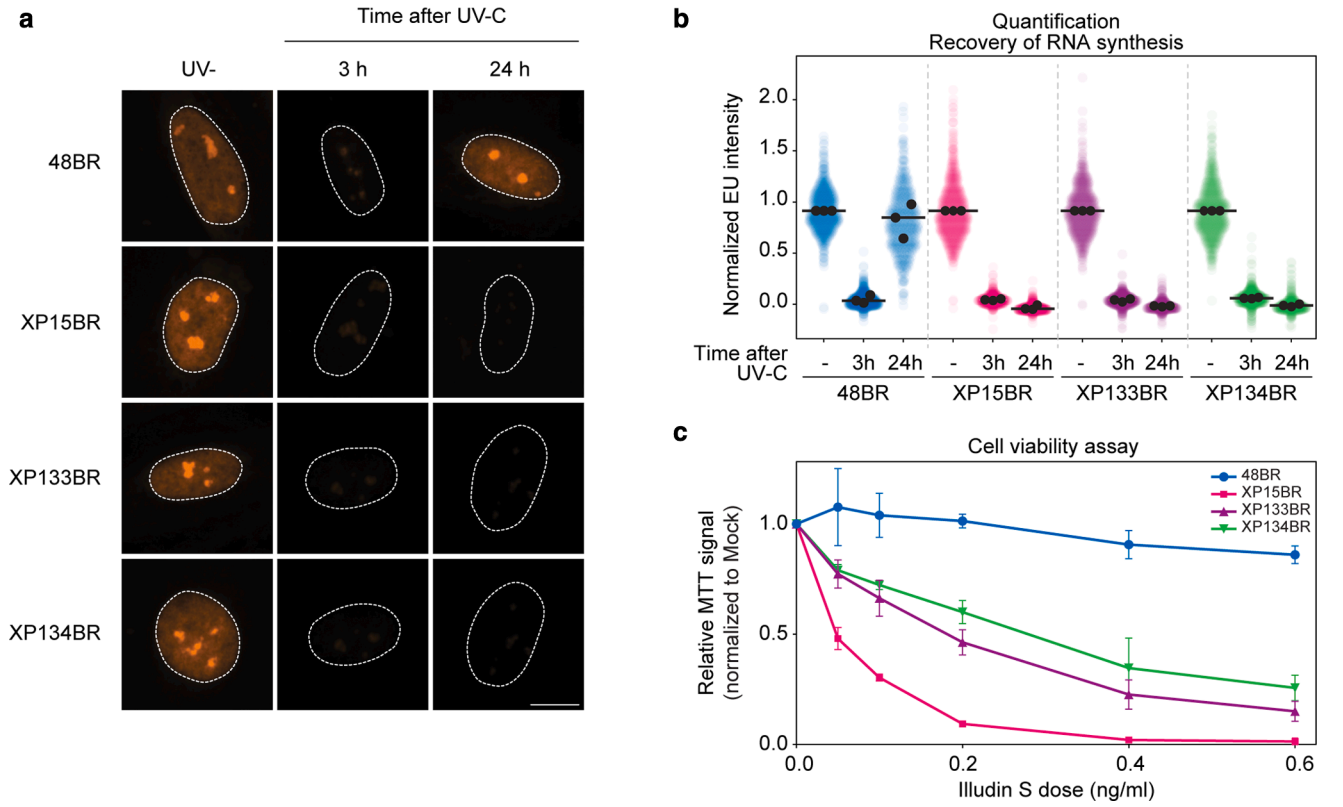

Figure 1. *XPA*$^{c.389G>A}$ variant results in significantly reduced TC-NER in patient-derived primary fibroblasts. (**a**) Representative images and (**b**) quantification of all results of the RRS assay in indicated control and patient-derived primary fibroblasts. Cells were either mock treated (UV-) or irradiated with 12 J/m^2 UV-C followed by pulse labeling with EU at the indicated time points. Images show EU staining in the nucleus, which are marked by a dashed line (on the basis of DAPI staining, not shown). Bar = 10 μm. (**c**) Quantification of an MTT cell viability assay after a 7-day treatment with different doses of Illudin S, an agent that induces transcription-blocking DNA lesions repaired by TC-NER. Error bars represent the SD of 3 technical replicates. Data are normalized per replicate to mock treatment (ie, treated with drug solvent only, DMSO). EU, 5-ethynyl-uridine; h, hour; RRS, recovery of RNA synthesis; TC-NER, transcription-coupled nucleotide excision repair.

parallel. These results suggest a strong TC-NER defect in the XP-A patient cells. To further confirm this, we assessed cell viability using an MTT assay after exposure to Illudin S, an agent that induces transcription-blocking DNA lesions repaired by TC-NER (van der Weegen et al, 2021). After 7 days of Illudin S exposure, XP133BR and XP134BR cells exhibited intermediate cell viability, whereas XP15BR cells were more sensitive to Illudin S treatment (Figure 1c). Together with the transcription recovery assay, these findings indicate a strong TC-NER defect in patient cells, although residual repair activity likely mitigates strong sensitivity to transcription-blocking damage.

Residual unscheduled DNA synthesis in patient cells

To measure GG-NER, we locally exposed cells to 30 J/m^2 UV-C through 5-μm pore filters and incubated them with the thymidine analog 5-ethynyl-deoxy-uridine (EdU) for 1 hour to measure unscheduled DNA synthesis (UDS) induced by the gap-filling DNA synthesis during DNA repair (van der Meer et al, 2023). UDS after UV irradiation is therefore primarily a measure of GG-NER activity. The level of UDS after UV irradiation was severely reduced in XP133BR and XP134BR patient cells, confirming the clinical diagnosis of XP (Figure 2a). When allowing cells to incorporate EdU at local damage sites for 4 hours, we detected some residual repair activity in the patient cells, which was not observed in XP15BR cells (Figure 2b). To extend these findings, we performed an MTT assay to measure cell viability in response to 4-nitroquinoline 1-oxide, a UV radiation-mimetic agent that induces purine adducts repaired by NER. After 7 days of 4-nitroquinoline 1-oxide exposure, XP133BR and XP134BR cells exhibited intermediate cell viability, whereas XP15BR cells were more sensitive to 4-nitroquinoline 1-oxide treatment (Figure 2c). These results are consistent with previous findings in XP3JO (GM02033) and XP4JO (GM02090) patient cells carrying the same variant as our patients (Satokata et al, 1992b) and suggest some residual GG-NER activity in patient cells, in line with their mild XP phenotype.

Nearly undetectable XPA protein in patient cells

We used immunoblotting to measure the amount of XPA protein in cell extracts. Surprisingly, we found very low levels of XPA protein in XP133BR and XP134BR cells, despite the predicted conservative amino acid substitution (Figure 2d). On the basis of published structures containing XPA, we propose that the p.R130K substitution would have a relatively modest effect and is unlikely to significantly alter the stability of the XPA protein or its ability to interact with DNA or RPA. To directly test this, we first knocked out XPA in RPE1-hTERT cells (XPA^{KO}) using CRISPR-Cas9 technology. Subsequently, we expressed a cDNA encoding either GFP-XPA^{WT} or GFP-XPA^{R130K} in the XPA^{KO} cells. Western blot analysis showed

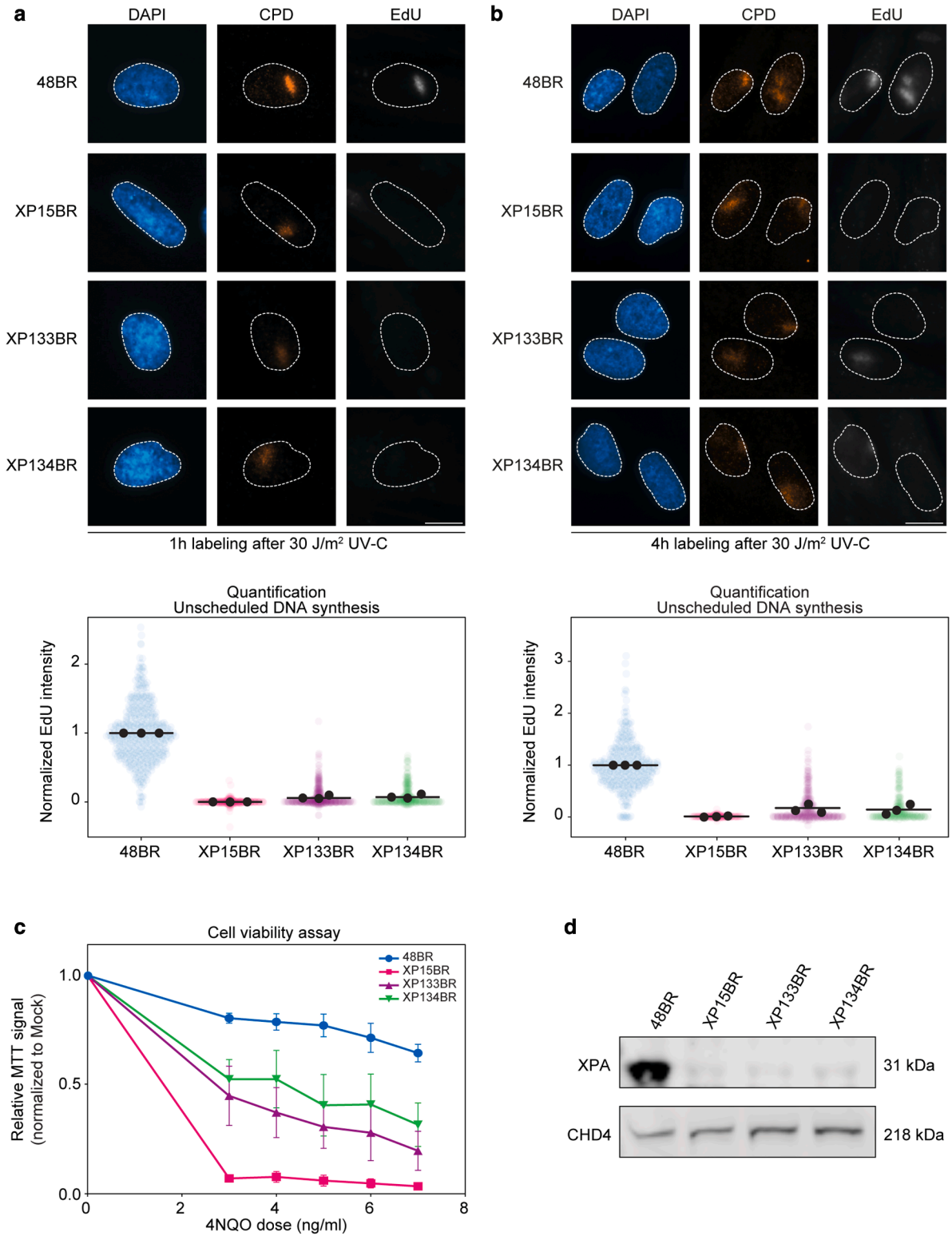

Figure 2. *XPA*$^{c.389G>A}$ variant results in significantly reduced GG-NER in patient-derived primary fibroblasts. (**a**) Representative images (top) and quantification of all results (bottom) of the 1-h EdU incorporation in the UDS assay. Sites of local damage are identified by CPD staining. (**b**) Same as in **a** but with 4-h EdU incorporation. (**a, b**) Bar = 10 μm. (**c**) Quantification of an MTT cell viability assay after a 7-day treatment with different doses of 4-NQO, a UVR-mimetic agent that induces purine adducts repaired by NER. Error bars represent the SD of 3 technical replicates. Data are normalized per replicate to mock treatment (ie, treated with drug solvent only, DMSO). (**d**) Analysis of XPA protein levels by western blot analysis in control (48BR) and patient-derived (XP15BR, XP133BR and XP134BR) fibroblasts. The levels of CHD4 serve as loading control. 4-NQO, 4-nitroquinoline 1-oxide; EdU, 5-ethynyl-deoxy-uridine; GG-NER, global genome nucleotide excision repair; h, hour; NER, nucleotide excision repair; UDS, unscheduled DNA synthesis; UVR, ultraviolet radiation; XP, xeroderma pigmentosum.

that the XPA^{R130K} protein variant was as stable as the XPA^{WT} protein (Supplementary Figure S1c). In addition, we purified recombinant XPA^{WT} and XPA^{R130K} proteins from *E coli*, along with the more disruptive amino acid substitution variant XPA^{R130I} (Blee et al, 2024). All XPA proteins were stable, suggesting that neither the conservative amino acid substitution nor the more disruptive XPA^{R130I} substitution destabilizes the XPA protein (Supplementary Figure S1d).

XPA^{R130K} is functional in NER

In further experiments, we functionally assessed the impact of the p.R130K substitution in XPA. Expression of XPA^{R130K} in XPA^{KO} cells fully rescued the strong UDS and RRS phenotypes observed in these cells to the same extent as re-expression of XPA^{WT} (Figure 3a–d). XPA^{R130K} or the more disruptive amino acid substitution variant XPA^{R130I} (Blee et al, 2024) retained its capacity to bind DNA in vitro (Figure 4a). We next measured NER excision activity in vitro by incubating purified XPA^{R130K} (and XPA^{R130I}) or XPA^{WT} with a plasmid containing a site-specific 1,3 GTG-Cisplatin lesion along with purified NER factors XPC-RAD23B, TFIIH, RPA, XPG, and ERCC1-XPF. Both protein variants supported in vitro NER to near wild-type levels (Figure 4b and c). Overall, our results show that XPA^{R130K} is not only stable but also fully functional in NER.

A splicing defect leads to reduced *XPA* transcript levels

Because the predicted amino acid substitution variant did not explain the observed XP disease pathology in both patients, we next focused on the location of the variant in the *XPA* gene. The mutated base in *XPA*, c.389G>A, is the last nucleotide of exon 3, and we hypothesized that this may cause abnormal splicing of *XPA* mRNA, explaining the low levels of XPA protein. To test this, we isolated mRNA from XP133BR and XP134BR patient cells and analyzed the presence of canonical or alternative *XPA* splice variants. End-point PCR analysis with primers targeting *XPA* between exons 1 and 5 identified 1 main *XPA* splice variant in cells with wild-type *XPA* (48BR). Fragment length and Sanger sequencing confirmed that this was the canonical *XPA* splice variant, including all exons 1–5 (Figure 5a and Supplementary Figure S2). However, in the patient cells with the *XPA*$^{c.389G>A}$ variant, this canonical splice variant was strongly reduced. Instead, we observed the formation of 2 alternative splice variants. Fragment length and Sanger sequencing analyses identified these variants as containing alternative splicing events that excluded exon 3 (splicing from exon 2 to exon 4) or exons 3–4 (splicing from exon 2 to exon 5), respectively. Thus, in the absence of an intact exon 3 splice donor site, the canonical splice donor site of exon 2 utilizes the canonical splice acceptor sites of exons 4 and 5, leading to the skipping of either exon 3 or exons 3 and 4.

Low levels of *XPA* transcript lead to ∼5% of functional XPA protein

qPCR analyses of the individual splice events confirmed that the canonical exon 2 to exon 3 splicing event was strongly reduced, to less than ∼5% (near the lower quantitative detection limit of our assay), in both *XPA*$^{c.389G>A}$ variant fibroblast lines (XP133BR and XP134BR) as compared to wild-type XPA cells (48BR) (Figure 5b). In contrast, both alternative splice events were strongly increased. Notably, the alternative splice event from exon 2 to exon 4 was almost exclusive to *XPA*$^{c.389G>A}$ variant fibroblasts, with nearly undetectable levels in 48BR (Figure 5b). Both alternative splice events result in a frameshift and the introduction of a premature stop codon. Excluding exon 3 results in a −1 nt frameshift and a premature stop codon after 12 amino acids, whereas excluding exons 3–4 results in a +1 nt frameshift and a premature stop codon after 7 amino acids. Even if such a truncated XPA protein were stable, which is unlikely, it would not be functional because it would lack essential regions involved in DNA binding and interaction sites with RPA or TFIIH (Kim et al, 2022; van den Heuvel et al, 2023).

Nonetheless, the residual UDS observed in the patient cells may result from the low but detectable amounts of normally spliced mRNA, leading to the XPA^{R130K} variant, which we have demonstrated has minimal impact on protein activity. To test this possibility, we revisited our western blot analysis of XPA protein levels shown in Figure 2d. To enable the detection of low levels of XPA protein, we loaded 25% (12.5 μg) or 10% (5 μg) of a wild-type cell lysate from 48BR cells and compared this with 50 μg of cell lysate from XP-A patient cells (Figure 5c). Although we still did not detect any residual XPA protein in cells from XP15BR, a severely affected patient with XP-A (Sethi et al, 2016), we detected low levels (∼5%) of XPA protein in cells from XP133BR and XP134BR. These low levels (∼5%) of functional XPA protein likely explain the relatively mild XP phenotype in these patients.

DISCUSSION

Our study provides insight into the nuanced relationship between genotype, splicing defects, and clinical presentation in patients with XP (XP-A). The 2 Cypriot patients, who share the homozygous variant c.389G>A (p.R130K) in the *XPA* gene, exhibit a relatively mild XP-A phenotype with distinct clinical outcomes. This variant, although associated with significantly reduced levels of XPA protein, does not compromise the intrinsic stability or functionality of the protein. Instead, the clinical and cellular abnormalities stem from an altered mRNA splicing pattern, highlighting the central role of transcriptional misregulation in determining phenotypic severity.

The older patient began to experience progressive neurological degeneration in his 40s, along with cutaneous symptoms, whereas the younger patient, still in her thirties, has so far exhibited only dermatological abnormalities. Notably, magnetic resonance imaging findings of cerebellar atrophy in the younger patient hint at subclinical neurodegeneration, underscoring the importance of longitudinal neurological monitoring in patients with XP-A with mild clinical presentations.

The cell biological and biochemical assays confirm that the p.R130K substitution does not inherently destabilize the XPA protein or impair its interaction with key NER components, as would be expected from a conservative R to K substitution. In vitro and cellular experiments demonstrate that XPA^{R130K} is fully capable of supporting NER activity, which contrasts with the low levels of functional NER observed in patient fibroblasts. This discrepancy is explained by abnormal splicing due to the mutation being positioned at the

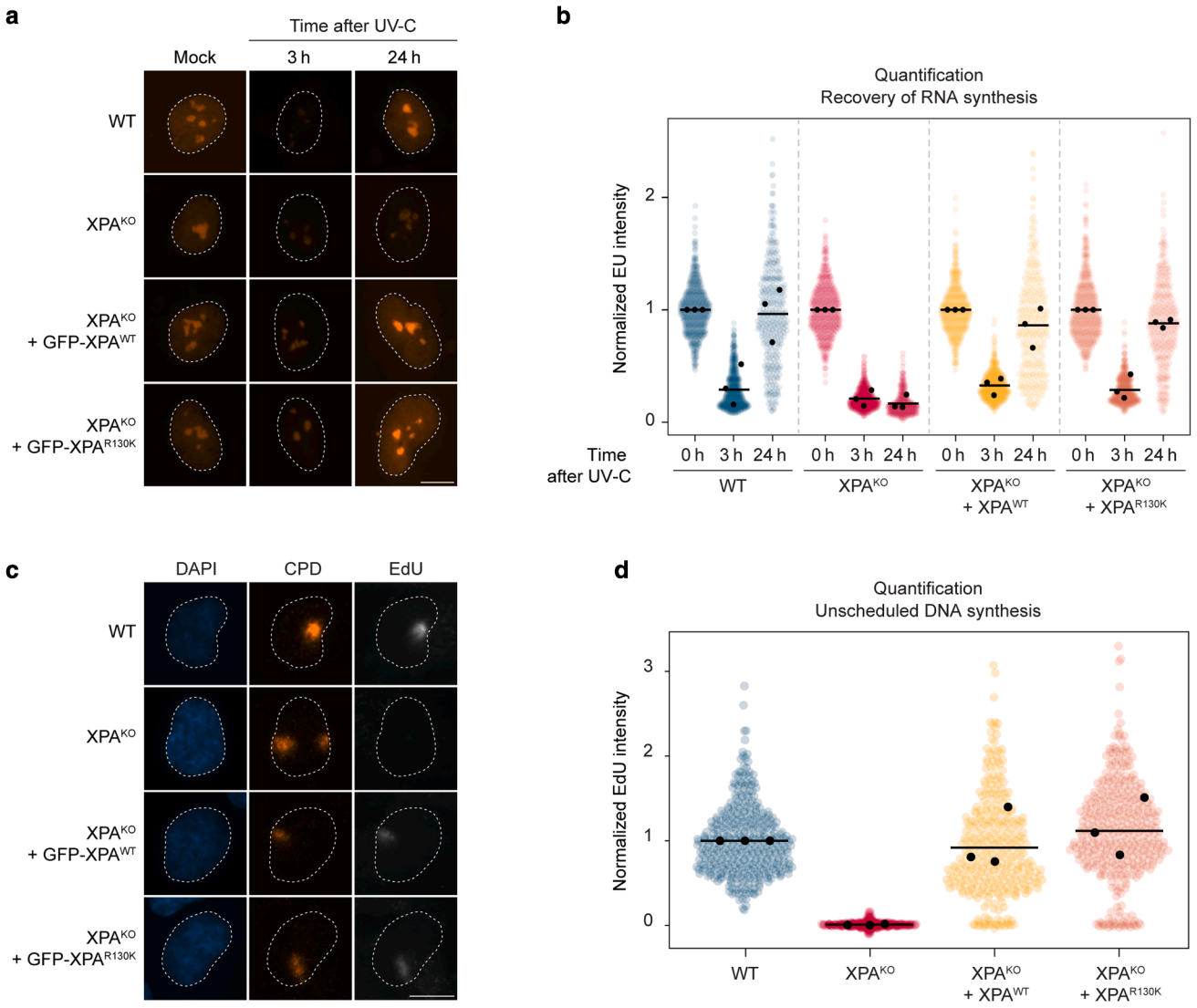

Figure 3. XPA^{R130K} variant rescues GG-NER and TC-NER in XPA^{KO} cells. (**a**) Representative images and (**b**) quantification of the RRS assay in the indicated RPE1-hTERT cells. Cells were either mock treated (UV-) or irradiated with 12−16 J/m^2 UV-C, followed by pulse labeling with EU at the indicated time points. Images show EU staining in the nucleus, marked by a dashed line (on the basis of DAPI staining, not shown). (**c**) Representative images and (**d**) quantification of the EdU incorporation in the UDS assay in the indicated RPE1-hTERT cells. Sites of local damage are identified by CPD staining. Bar = 10 μm. EdU, 5-ethynyl-deoxy-uridine; EU, 5-ethynyl-uridine; GG-NER, global genome nucleotide excision repair; h, hour; RRS, recovery of RNA synthesis; TC-NER, transcription-coupled nucleotide excision repair; UDS, unscheduled DNA synthesis; WT, wild type; XP, xeroderma pigmentosum.

exon−intron boundary at the 3′ end of exon 3. This abnormal splicing results in significantly reduced levels of the canonical *XPA* splice variant, associated with an increased production of 2 alternative *XPA* splice variants (exons 2−4 and exons 2−5), with the exon 2 to exon 4 splice variant being near exclusive to the *XPA*$^{c.389G>A}$ variant cells. Both alternative splice events result in a frameshift and the introduction of a premature stop codon, which generally renders the transcripts susceptible to degradation through the nonsense-mediated decay pathway. This may explain the low XPA protein levels. Alternatively, any stable mRNA containing such a premature stop codon could lead to the production of either an unstable XPA protein or a stable but nonfunctional form lacking essential domains.

Similar observations were made in cells from 2 patients with the same variant as our patients (Satokata et al, 1992b). Both patients are of African descent, with patient XP4JO showing skin hypo- and hyperpigmentation without malignancies. Fibroblasts from these patients exhibited intermediate UV sensitivity and markedly reduced *XPA* mRNA levels. Specifically, there was a decrease in normally spliced mRNA and an increase in mRNA lacking exon 3 due to aberrant splicing. Our findings support and extend these observations by demonstrating that despite this splicing defect, low levels of XPA^{R130K} protein are still produced, likely providing partial protection against the development of severe XP.

Quantitative immunoblotting suggests that the level of XPA protein in our patients' fibroblasts is <5% of that in normal fibroblasts. Residual functional protein appears sufficient to confer some NER activity, as evidenced by the limited but detectable UDS and global genome repair observed in

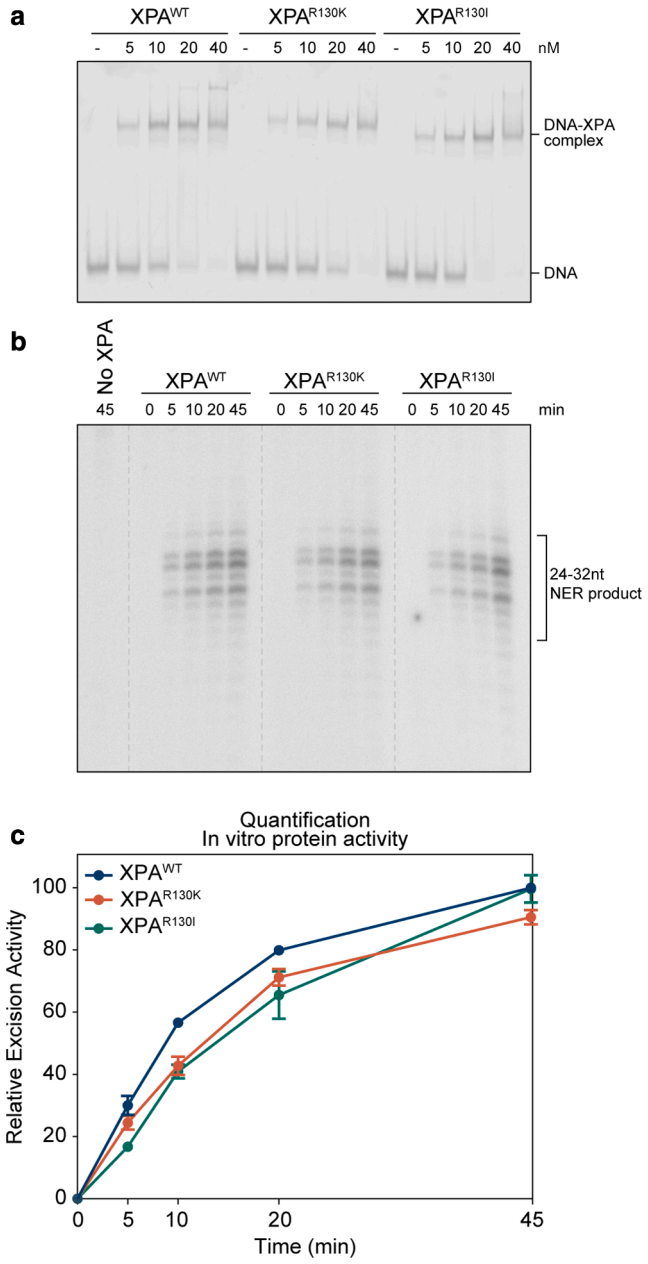

Figure 4. XPA^{R130K} retains normal DNA-binding capacity and NER activity. (**a**) EMSA of XPA^{WT}, XPA^{R130K}, and XPA^{R130I} for DNA-binding affinity. Three-way junction DNA substrate was incubated with indicated amounts of XPA (wild-type or variants) for 30 minutes. (**b**) In vitro NER assay of XPA (wild type or variants). A plasmid containing a site-specific cisplatin lesion was incubated with purified 20 nM XPA (wild type or variants), 5 nM XPC-RAD23B, 10 nM TFIIH, 42 nM RPA, 27 nM XPG, and 13 nM XPF-ERCC1 for the indicated time. The excision products were detected by annealing to a complementary oligonucleotide with a 4dG overhang, which was used as a template for a fill-in reaction with [α-32P] dCTP. (**c**) Quantification of the in vitro NER assay in **b**. Band intensity was normalized to XPA^{WT} product at 45 minutes. The data represent 2 independent experiments. EMSA, electrophoresis mobility shift assay; min, minute; NER, nucleotide excision repair; XP, xeroderma pigmentosum.

patient cells. This aligns with the relatively mild cutaneous manifestations and delayed neurological degeneration compared with classic XP-A cases with complete loss of XPA function. Indeed, mild clinical features have also been reported in patients with XP-C with splice variants that result in low *XPC* transcript levels (Khan et al, 2010, 2004). Nevertheless, the severe TC-NER defect may underlie the neurological phenotype in the older patient with XP-A, consistent with prior findings linking TC-NER deficiency to neurodegeneration (Calmels et al, 2018; Laugel et al, 2010; Lehmann, 2003; van den Heuvel et al, 2023). Similarly, some patients with XPD or XPF variants exhibit adult-onset neurological degeneration (Cordts et al, 2022; Fassihi et al, 2016), which may be an underdiagnosed cause of neurodegeneration in adults.

Our findings add to a growing body of evidence showing how variants in splice site sequences can result in unanticipated clinical phenotypes in the *XPA* gene. Mutations at the invariant splice donor GT or splice acceptor AG generally result in 100% mis-splicing and a lack of functional protein. This, as exemplified by the Japanese founder effect (ENST00000375128.5:c.390-1G>C), confers a very severe clinical phenotype (Satokata et al, 1990). However, we recently described a cohort of patients originating from the Indian subcontinent who contained a variant near the splice donor site for intron 4 (ENST00000375128.5:c.555+8A>G) (Sethi et al, 2016). This resulted in abnormal splicing of the majority of *XPA* mRNA, but the approximately 5% of residual and normally spliced mRNA generated sufficient XPA protein to ameliorate the skin symptoms and completely prevent the neurological degeneration (Sethi et al, 2016; Sidwell et al, 2006). A study by Sagun et al (2024) recently described 2 additional patients with this intron 4 variant as well as 5 patients with a variant at the last base of exon 4 (ENST00000375128.5:c.555G>C; ENSP00000364270.5:p.Q185H). The 1 patient homozygous for this exon 4 variant, first identified by Satokata et al (1992b), had intermediate neurological problems. We suspect that the mRNA species with an in-frame deletion of 6 bp or with a 36-bp insertion at the beginning of intron 4 may permit some residual XPA activity in this patient.

Our findings together with those reported elsewhere illustrate how residual NER activity, driven by minimal amounts of functional protein, can ameliorate neurological outcomes in XP. In addition, our work highlights the importance of considering splicing effects in variant analysis because even conservative amino acid changes may lead to profound phenotypic consequences through post-transcriptional mechanisms. Future studies investigating splicing modulators or therapeutic strategies to enhance mRNA levels could hold promise for managing patients with XP-A with splicing defects.

This study underscores the complexity of XP-A pathogenesis, where subtle molecular disruptions can yield diverse clinical outcomes. The interplay between genotype, mRNA splicing, and cellular repair capacity emphasizes the need for comprehensive molecular and clinical assessments to guide prognosis and intervention in patients with XP-A.

MATERIALS AND METHODS

Subjects

This study describes 2 unrelated Cypriot patients with XP-A with a mild phenotype linked to a homozygous missense variant in *XPA* (ENST00000375128.5:c.389G>A, ENSP00000364270.5:p.R130K). Materials from the included patients are referred to as XP133BR (a female aged 32 years) and XP134BR (a male aged 69 years). Detailed

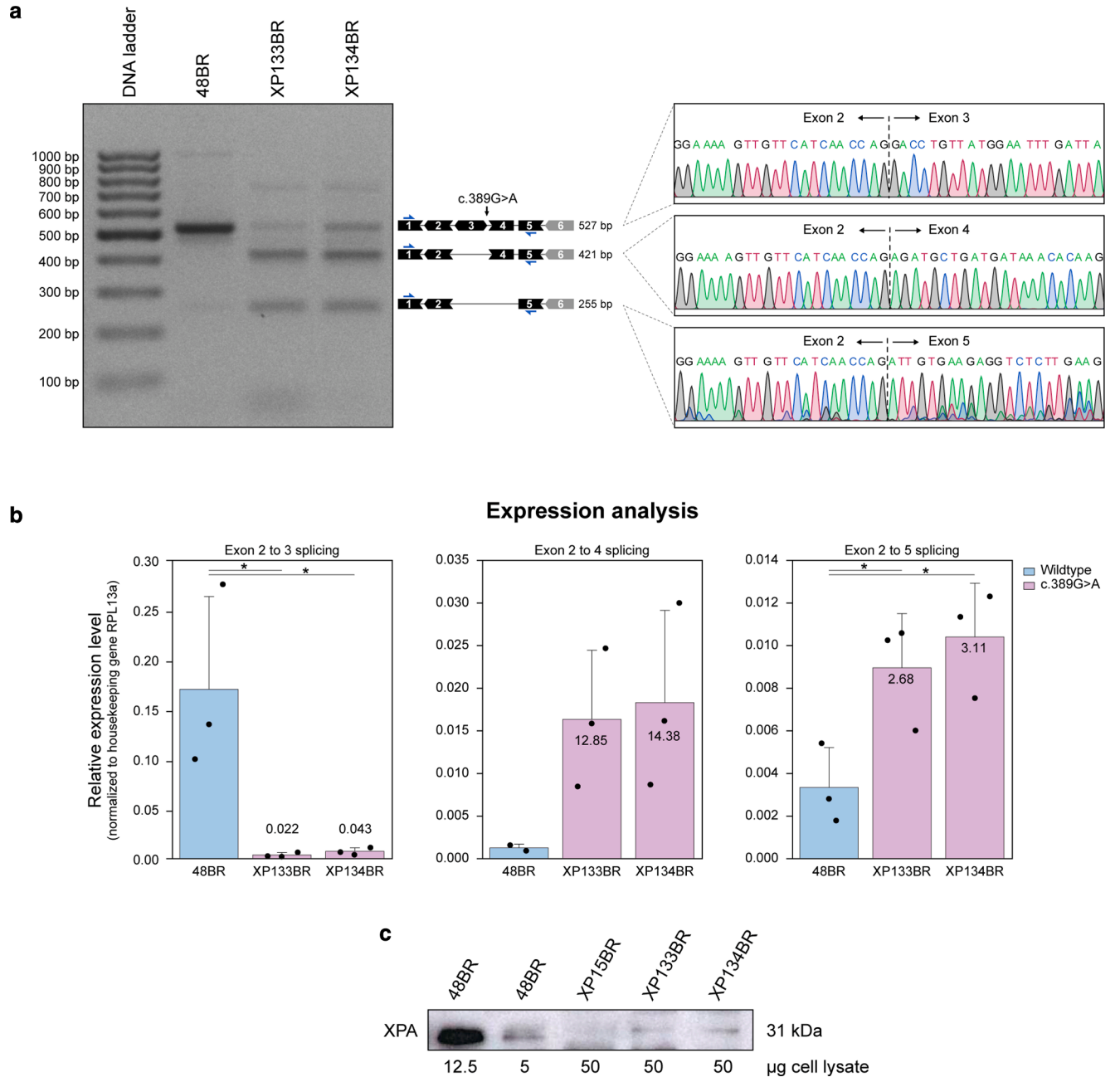

Figure 5. *XPA*$^{c.389G>A}$ results in alternative *XPA* splicing with significantly reduced levels of canonical (functional) XPA. (**a**) Fragment length analysis (left, agarose gel electrophoresis) and Sanger sequencing results (right) of an endpoint PCR of the *XPA* splice variants expressed in control (48BR) and patient-derived (XP133BR and XP134BR) primary fibroblasts. A schematic representation of each produced splice variant is depicted at each PCR product. The position of the c.389G>A variant and the location of the used primers (blue arrows) are indicated. Exon 6 is colored in gray because it was not included in this splicing analysis. (**b**) RT-qPCR analysis results of the canonical *XPA* splice variant (exons 2−3) and the 2 main alternative *XPA* splice variants (exons 2−4 and exons 2−5). Bars represent the mean expression level of 3 replicates, with the error bars depicting the SD. Black points depict the results of the individual replicates. Values are normalized to the expression level of housekeeping gene *RPL13a*. Values in the bars indicate the fold change in the patient-derived fibroblasts over the control fibroblasts (48BR). *P*-values depict the results of a 1-way ANOVA with Dunnett's multiple comparison test, comparing both XP133BR and XP134BR with the control 48BR, with $*P < .05$ and $**P < .01$ (tested but not observed). Statistics for exons 2−4 variants are not included because expression in XPA^{WT} cell line was too low for accurate quantitative analysis. (**c**) Western blot analysis of XPA protein levels in control (48BR) and patient-derived XP15BR, XP133BR, and XP134BR fibroblasts. To detect lower, residual XPA protein levels, 12.5 µg and 5 µg cell lysates from wild-type 48BR cells were mixed with 37.5 µg and 45 µg cell lysates from XPA-deficient XP15BR cells, loaded, and compared with 50 µg cell lysate of patient fibroblasts. XP, xeroderma pigmentosum.

description of clinical characteristics per patient are described in the results section. All patients provided written informed consent to participate in the study, for the use of their clinical data and photographs, and for the generation of primary fibroblast cell lines. The ethnicity of participants was identified by the medical team at the National Xeroderma Pigmentosum Service in London. These data were collected because disease prevalence, severity, and clinical outcomes vary significantly between populations, influencing the development of preventive strategies and tailored patient care.

Variant nomenclature

All variants reported and discussed in this study are reported based on the following XPA reference sequences: Ensembl Gene-ID ENSG00000136936, Ensembl Transcript-ID ENST00000375128.5 and/or Ensembl Protein-ID ENSP00000364270.5.

Cell lines

The cell lines used in this study were cultured at 37 °C and 5% carbon dioxide. Human primary fibroblasts were cultured in DMEM supplemented with GlutaMAX (Gibco, catalog number 31966-047), 20% fetal calf serum (FCS) (Biowest, catalog number S1600), and 1% penicillin/streptomycin. Patient fibroblasts were obtained from skin biopsies. In addition, RPE1 (retinal pigment epithelial) cell line and variants were cultured in DMEM supplemented with GlutaMAX, 8% FCS, and 1% penicillin/streptomycin. All cell lines used are listed in Supplementary Table S1.

MTT assay for cell viability

Primary fibroblasts were seeded in 96-well plates at a density of 1000 cells per well. Directly starting at plating, cells were incubated with different doses of Illudin S (Santa-Cruz Biotechnology, sc-391575, dissolved in DMSO) or 4-nitroquinoline 1-oxide (Sigma-Aldrich, N8141-250MG, dissolved in DMSO) in a total medium volume of 200 μl/well. Cells were incubated for 7 days at 37 °C in a humidified incubator with 5% carbon dioxide. On the final day, the medium was removed and replaced with 80 μl of fresh DMEM supplemented with 8% FCS, followed by 20 μl of MTT solution (Thermo Fisher Scientific, catalog number M6494, 5 mg/ml in PBS). Plates were protected from light and incubated for 1.5–2.5 hours at 37 °C with gentle shaking. After incubation, the medium was carefully removed, and 200 μl DMSO was added to each well to solubilize the purple formazan crystals. Plates were gently mixed at room temperature for 5 minutes. Absorbance was measured at 570 nm using a SpectraMax ID3 plate reader.

Plasmids

A region spanning the PGK promoter was amplified by PCR and used to replace the CMV promoter in pEGFP-C1-IRES-PURO (previously described in Typas et al [2015]). Overlap PCR was used to generate EGFP-XPA with amino acid substitution R130K (forward primer oML#120 GCCAACTTGTGATAACTGCAAAGATGCTGATGA TAAACAC). The XPA^{WT} and XPA^{R130K} genes were inserted into pPGK-EGFP-C1-IRES-PURO. All plasmids used are listed in Supplementary Table S2.

Generation of RPE1-hTERT knockout and rescue cells

Parental RPE1-hTERT cells stably expressing iCas9 (inducible Cas9) that are also knockout for *TP53* and the puromycin-N-acetyltransferase *PAC1* gene were described previously (referred to as RPE1-iCas9) (van der Weegen et al, 2021). RPE1-iCas9 cells were cotransfected with 3 μg pU6-sgXPA-PGK-puro-2A-tagBFP (Sigma-Aldrich library from the Leiden University Medical Center, described in van den Heuvel et al [2023]) and 3 μg pX458 (Addgene) encoding Cas9 in 3.6 ml optiMEM with 10% FCS and 6 μl lipofectamine 2000 (Thermo Fisher Scientific). Cells were FACS sorted on BFP/EGFP and plated at low density, after which individual clones were isolated, expanded, and verified by western blot analysis and/or Sanger sequencing. An RPE1 clone that was verified to be knockout for XPA (clone 1) was transfected with either pPGK-EGFP-XPA^{WT}-IRES-PURO or pPGK-EGFP-XPA^{R130K}-IRES-PURO. Cells were selected with 1 μg/ml puromycin to generate a polyclonal stable cell line. Homogeneous expression of EGFP-XPA proteins was verified by western blot analysis.

Western blot

Whole-cell lysates were obtained by washing cells with PBS and adding Laemmli buffer (40 mM Tris pH 6.8, 3.35% SDS, 16.5% glycerol, 0.0005% bromophenol blue, and 0.05 M DTT) or by resuspending cell pellets (250,000 cells) in PBS, spinning them down for 5 minutes at 1500 rcf, and then resuspending them in Laemmli buffer. All samples were heated for 15 minutes at 98 °C to denature proteins. The samples were loaded on a 4–12% Criterion XT Bis-Tris gel (Bio-Rad Laboratories, catalog number 345-0124) with a Precision Plus Protein Ladder (Bio-Rad Laboratories, catalog number 1610374). The gel was run for 15 minutes at 75 volts and then increased to 120 volts until the bands were sufficiently separated. Before transfer, the membrane (Immobilon-FL PVDF, Merck Millipore, catalog number IPFL00010) was activated with methanol, and proteins from the gel were transferred to the membrane at 50 volts for 2 hours at 4 °C in blot buffer (25 mM Tris, 192 mM glycine, and 20% [v/v] methanol in deionized water). The membrane was blocked with blocking buffer (5% skimmed milk powder in PBS-$Tween_{0.1\%\ [v/v]}$) or commercial blocking buffer (Rockland Immunochemicals, catalog number MB-070-010) for 1 hour at room temperature while shaking. Proteins were visualized by incubating the membrane overnight with primary antibodies in blocking buffer, followed by 4 washes with PBS-$Tween_{0.1\%\ (v/v)}$ and a 1-hour incubation in the dark with secondary antibodies (Supplementary Table S3 presents antibody details). Finally, the membrane was washed 4 times with PBS-$Tween_{0.1\%\ (v/v)}$, and proteins were detected using the Odyssey CLx system. Blots were analyzed using Image Studio Lite.

Local UDS assay

To measure DNA repair-related synthesis, we measured UDS after inducing local UV damage. First, for patient-derived primary fibroblast cells, 180,000 cells were seeded onto 18-mm coverslips in DMEM Glutamax, supplemented with 20% FCS and 1% penicillin/streptomycin. For RPE cell lines, 100,000 cells were seeded onto 18-mm coverslips in DMEM Glutamax, supplemented with 8% FCS and 1% penicillin/streptomycin. Starvation medium (DMEM Glutamax with 1% penicillin/streptomycin) was added to both cell types the following day. After at least 24 hours, the cells were washed twice with PBS followed by local irradiation with 30 J/m^2 UV-C through a Polycarbonate Membrane Filter with 5.0 μm Pore Size (Millipore, catalog number TMTP04700) to create local DNA lesions. The cells were incubated for either 1 hour or 4 hours at 37 °C with an EdU/5-fluoro-2′-deoxyuridine mix (50 μM EdU, Jena Bioscience, catalog number CLK-N001-100) and 1 μM 5-fluoro-2′-deoxyuridine (Sigma-Aldrich, catalog number F0503) in DMEM Glutamax + 1% penicillin/streptomycin. EdU is incorporated into DNA in place of thymidine. Cells were then chased for 15–30 minutes at 37 °C with 10 μM thymidine (Sigma-Aldrich, catalog number T1895-1G) in plain DMEM Glutamax. Afterward, cells were fixed with 3.7–4% formaldehyde (Sigma-Aldrich, catalog number 252549-500ML) for 15 minutes at room temperature and washed twice with PBS. Cells were permeabilized with 0.5% Triton-X100 (Sigma-Aldrich, catalog number X100) for 20 minutes in the dark, washed twice with PBS + 3% BSA (Sigma-Aldrich, catalog number 10735086001), and washed once with PBS. EdU incorporation was visualized using a click chemistry mix (40 mM Tris, pH 8, 60 μM Attoazide Alexa 647 [Atto Tec, catalog number 647N-101], 4 mM copper(II) sulfate

[VWR International, catalog number 23174.233], and 10 mM L-ascorbic acid [Sigma, catalog number A0278-100G]) and incubated for 30 minutes at room temperature in the dark. Cells were washed with PBS, postfixed with 2% formaldehyde for 10 minutes in the dark, washed with PBS twice, and blocked with 100 mM glycine (Sigma-Aldrich, G7126-5KG) for 10 minutes in the dark to prevent signal loss. DNA was denatured for 5 minutes with 0.5 M sodium hydroxide (Sigma-Aldrich), washed with PBS 3 times, and blocked again with PBS + 10% BSA for 15 minutes in the dark. Cells were washed twice with PBS, followed by 1 wash with PBS + 0.5% BSA + 0.05% (v/v) Tween-20, and incubated for 2 hours at room temperature with primary antibodies in wash buffer (PBS + 0.5% BSA + 0.05% Tween-20). Cells were washed 4 times with wash buffer and incubated with secondary antibodies for 1 hour at room temperature in the dark (Supplementary Table S3 presents antibody details). DAPI (Merck, D8417-1MG) was added for 5 minutes, and coverslips were mounted on microscopy slides with Aqua Polymount (Brunschwig, catalog number 18606) after the final PBS washes.

RRS assay

To measure RNA synthesis after irradiation, 40−80,000 cells were seeded on 12-mm coverslips. The next day, cells were starved for at least 24 hours in starvation medium (DMEM Glutamax + 1% FCS + 1% penicillin/streptomycin). Cells were washed with PBS and irradiated with 12−16 J/m^2 UV-C, after which starvation medium was reintroduced, and the cells were incubated at 37 °C. RNA synthesis was measured at various time points (mock, 3 hours, and 24 hours after UV-C) by incubating the cells with 400 μM EU (Jena Bioscience, catalog number CLK-N002-10), a uridine analog, in DMEM Glutamax + 1% FCS for 1 hour at 37 °C. Afterward, cells were washed and chased for 15−30 minutes in DMEM Glutamax + 1% penicillin/streptomycin at 37 °C. Cells were fixed with 3.7−4% formaldehyde for 15 minutes at room temperature and washed twice with PBS. Permeabilization was done using 0.5% Triton-X100 for 10 minutes, and blocking was done using PBS + 1.5% BSA for 10 minutes. To visualize the EU, coverslips were incubated for 1 hour in the dark with a click-it mix (40 mM, Tris pH 8, 60 μM Attoazide Alexa 594 [Atto Tec, catalog number 647N-101], 4 mM copper[II] sulfate, 10 mM L-ascorbic acid, and DAPI 1:1000). After 5 PBS washes, coverslips were mounted on microscopy slides using Aqua Polymount.

Data Analysis

Cells fixed, stained and mounted on slides during UDS and RRSs were imaged using a Zeiss AxioImager M2 wide-field fluorescence microscope with an HXP 120 metal-halide lamp for excitation and ×63 magnification. The magnification was achieved using ×63 PLAN APO (1.4 numeric aperture) oil-immersion objectives (Zeiss). Images were taken using ZEN pro 3.3 or ZEN 2012 software. DAPI, Alexa Fluor 555, and Alexa Fluor 647 channels were used to capture images of the cells. Images were analyzed with ImageJ software to measure the fluorescent signal intensity across different channels. Nuclei between 10.0 and 30.0 units were identified using the DAPI channel for all assays. For UDS assays, ImageJ's Li threshold was used to select nuclei (DAPI channel) and ImageJ's Yen threshold was used to select foci of DNA lesions (Alexa Fluor 555 channel, CPD signal). Foci between 1 and 60−100 units were selected, and those with outlier CPD intensity were excluded. EdU signal in the Alexa Fluor 647 channel was measured in damaged and undamaged regions. Cells undergoing scheduled DNA synthesis (S-phase) were excluded from analysis by setting a maximal mean and SD for EdU signal in undamaged regions. The mean background EdU intensity in the undamaged region was subtracted from that in the damaged region. EdU intensity was normalized to wild-type 48BR for patient fibroblasts and to RPE wild-type for RPE cell lines. For RRS assays, EU signal in the Alexa Fluor 555 channel was measured in nuclei, with the median background EU signal outside nuclei subtracted from the mean nuclear EU signal. For each condition, EU intensity was normalized to the mock-treated condition for the same cell line. Violin-dot plots of individual normalized data points were generated using PlotsOfData (Postma and Goedhart, 2019), with the mean represented by a black bar. The mean of individual experiments was added as black data points. Representative microscopy images were selected and shown in figures.

Expression and purification of XPA proteins

Wild-type or mutant full-length XPA with an N-terminal His_6 tag was expressed in *E coli* Rosetta pLysS cells. Cells were grown in LB medium containing 50 μg/ml kanamycin to optical density$_{600}$ = 0.6 at 37 °C and then to optical density$_{600}$ = 1.2 at 18 °C, followed by induction with 1 mM isopropyl β-D-thiogalactoside at 18 °C overnight. Cells were collected by centrifugation at 6500 r.p.m. for 20 minutes, and all subsequent purification steps were performed at 4 °C. The cell pellet from 1 l of culture was resuspended in 20 ml of lysis buffer (100 mM Tris-hydrogen chloride at pH 8.0, 500 mM sodium chloride, 20 mM imidazole, 5 mM 2-mercaptoethanol, 10 μM zinc chloride, 200 μg/ml lysozyme, 0.5 mM phenylmethylsulfonyl fluoride, 1 mM benzamidine, and 10% glycerol, and protease inhibitor [Roche]). The suspended pellets were Dounce homogenized 20 times and sonicated with an amplitude of 30 (5 seconds on/10 seconds off) for 2 minutes. The lysate was clarified by centrifugation at 20,000 r.p.m. for 40 minutes and filtration of the supernatant through a 0.45-mm syringe filter. The supernatant was incubated for 90 minutes at 4 °C with 2 ml of Ni-resin pre-equilibrated with Ni-loading buffer (100 mM Tris-hydrogen chloride, pH 8.0, 500 mM sodium chloride, 10 mM imidazole, 5 mM 2-mercaptoethanol, 10 μM zinc chloride, and 10% glycerol). The resin was washed twice with Ni-wash buffer (100 mM Tris-hydrogen chloride pH 8.0, 500 mM sodium chloride, 30 mM imidazole, 5 mM 2-mercaptoethanol, 10 μM zinc chloride, and 10% glycerol) and eluted with Ni-elution buffer (100 mM Tris-hydrogen chloride, pH 8.0, 500 mM sodium chloride, 250 mM imidazole, 5 mM 2-mercaptoethanol, 10 μM zinc chloride, and 10% glycerol). The eluent was applied to a 1 ml Hi-trap heparin column equilibrated with Hep-buffer (20 mM Tris-hydrogen chloride, pH 8.0, 50 mM sodium chloride, 5 mM 2-mercaptoethanol, 10 μM zinc chloride, and 10% glycerol) and eluted using a linear gradient with Hep/NaCl-buffer (20 mM Tris-hydrogen chloride, pH 8.0, 1.5 M sodium chloride, 5 mM 2-mercaptoethanol, 10 μM zinc chloride, and 10% glycerol) over 5 column volumes. The XPA protein was eluted at approximately 800 mM sodium chloride. The proteins were further purified on a HiLoad 16/600 Superdex 75 pg column with buffer (50 mM Tris-hydrogen chloride at pH 8.0, 150 mM sodium chloride, 1 mM dithiothreitol, 10 μM zinc chloride, and 10% glycerol), where they were eluted at 50−60 ml. The proteins were obtained at a concentration of ∼0.63 mg/ml, yielding a total of 2.5 mg per liter of cell culture.

In vitro NER activity assay with purified proteins

A plasmid containing a 1,3 GTG-Cisplatin lesion was incubated with purified NER protein (5 nM of XPC-RAD23B, 10 nM of TFIIH, 20 nM of XPA, 41.6 nM of RPA, 27 nM of XPG, and 13.3 nM of XPF-ERCC1). All proteins were >95% pure and produced as previously

described: XPC-RAD23B (Cheon et al, 2019), TFIIH (Gradia et al, 2017), RPA (Brosey et al, 2009), XPG (Hohl et al, 2003), and ERCC1-XPF (Enzlin and Schärer, 2002). The reactions were carried out in repair buffer containing 45 mM 4-(2-hydroxyethyl)-1-piperazineethanesulfonic acid potassium hydroxide, pH 7.8, 5 mM magnesium chloride, 0.3 mM EDTA, 40 mM phosphocreatine (di-Tris salt, Sigma-Aldrich), 2 mM ATP, 1 mM DTT, 2.5 μg BSA, 0.5 μg creatine phosphokinase (Sigma-Aldrich), and sodium chloride (to a final concentration of 70 mM) and 50 nM of purified wild-type or mutant XPA in a total volume of 9 μl were prewarmed at 30 °C for 10 minutes. A total of 1 μl of plasmid containing AAF (25 ng/μl) was added to reaction mixture and incubated at 30 °C for different incubation times (0, 5, 10, 20, 45, and 90 minutes). A total of 0.5 μl of 1 μM of a 3′-phophorylated oligonucleotide for product labeling was added, and the mixture was heated at 95 °C for 5 minutes. The mixture was allowed to cool down to room temperature for 15 minutes. A total of 1 μl of a Sequenase/[α-^{32}P]-dCTP mix (0.25 units of Sequenase and 2.5 μCi of [α-^{32}P]-dCTP per reaction) was added, and the mixture was incubated at 37 °C for 3 minutes. Then 1.2 μl of dNTP mix (100 μM of each dATP, dTTP, dGTP; 50 μM dCTP) was added to the mixture and incubated for another 12 minutes. The reactions were stopped by adding 12 μl of loading dye (80% formamide/10 mM EDTA) and heating at 95 °C for 5 minutes. A total of 6 μl of sample was loaded on 14% sequencing gel (7 M urea, 0.5× TBE) at 45 W for 2.5 hours. The reaction products were visualized using a PhosphorImager (Amersham Typhoon RGB, GE Healthcare Bio-Sciences). Two independent experiments were performed. The NER products were quantified using ImageQuant TL and normalized to the amount of NER product formed with XPA^{WT} at 90 minutes.

Electrophoretic mobility shift assay

Electrophoretic mobility shift assay was conducted using 3-way junction substrate as described in our previous paper (Topolska-Woś et al, 2020). The annealed 3-way junction oligonucleotides (10 nM) with fluorescein-label were incubated with wild-type or mutant XPA (0, 5, 10, 20, 40 nM) in a 10-μl mixture containing 25 mM Tris-hydrogen chloride (pH 8.0), 1 mM DTT, 0.1 mg/ml BSA, 5% glycerol, and 1 mM EDTA at 25 °C for 30 minutes. The reaction mixture was loaded onto 8% native polyacrylamide gel and run at 4 °C for 2 hours at 20 mA with 0.5% TBE buffer. Gels were scanned using an Amersham Typhoon RGB imager.

Expression analysis of XPA splice variants

To analyze *XPA* alternative RNA splicing events, total RNA was harvested from ∼300,000 patient-derived primary fibroblasts. For this, cells were cultured in 6-well format until ∼300,000 cells in DMEM Glutamax + 20% FCS + 1% penicillin/streptomycin. Cells were trypsinized, pelleted by centrifugation for 5 minutes at 1500 rcf, and lysed in 1 ml Trizol (Thermo Fisher Scientific, catalog number 15596018) for 5 minutes at room temperature. A total of 200 μl Chloroform (Thermo Fisher Scientific, catalog number 043685.K2) was added, and samples were vigorously mixed and incubated for 10 minutes at room temperature. Samples were centrifuged at 16,000 rcf for 20 minutes to induce phase separation. The upper aqueous phase (∼500 μl) was transferred to a new tube, and RNA was precipitated by adding 500 μl isopropanol (Boom, catalog number 61008067.1000), incubating the samples for 10 minutes and centrifuging them for 20 minutes at 16,000 rcf at 4 °C. RNA pellets were washed with 1 ml 75% (v/v) ethanol, centrifuged for 5 minutes at 16,000 rcf at 4 °C, air dried, and resuspended in 20 μl RNAse-free water. Potential contaminating genomic DNA was removed by incubating the RNA with 1:10 volumes of rDNAse I reaction mixture (1/10 dilution of rDNAse I in rDNAse I buffer [Machery-Nagel, catalog number 740963]) for 30 minutes at room temperature. DNAseI-treated RNA was purified with the RNeasy MinElute Cleanup kit (Qiagen, catalog number 74204) following the manufacturer's instructions, with a final elution volume of 14 μl. First-strand cDNA synthesis of 750 ng RNA per sample was performed with the RevertAID H-Minus First Strand cDNA synthesis kit (Life Technologies, catalog number K1632), following the manufacturer's instructions.

End-point PCR analysis of *XPA* splice variants was performed on ∼1 ng cDNA with Phusion High-Fidelity DNA Polymerase (New England Biolabs, catalog number M0530L), following the manufacturer's instructions, except for the addition of 3% (v/v) DMSO to the PCR reaction mix, and using 40 cycles of the following PCR program: denaturation at 98 °C for 10 seconds, annealing at 56 °C for 30 seconds, and extension at 72 °C for 60 seconds. Primers targeted *XPA* at respectively exon 1 and 5. All primers used in this study are provided in Supplementary Table S4. PCR products were run on a 1% (w/v) agarose gel containing 100 μg/l ethidium bromide (Santa Cruz Biotechnologies, catalog number SC-286960) and imaged with an Intas gel imager. For Sanger sequencing—based validation of the splice variants, bands were cut from the agarose gel, extracted with the QIAquick Gel Extraction kit (Qiagen, catalog number 28706), and analyzed by Sanger sequencing (Macrogen) using the primers used for the PCR amplification. Results were analyzed with ApE (version 3.0.8) (Davis and Jorgensen, 2022).

qPCR analysis of cDNA (ie, RT-qPCR) was performed with iQ SYBR Green Supermix (Bio-Rad Laboratories, catalog number 1708880), according to the manufacturer's instructions. Per reaction, ∼7.5 ng of cDNA was used. All RT-qPCRs included a 2-step PCR program of 40 cycles of denaturation at 95 °C for 10 seconds and annealing/extension at 60 °C for 30 seconds, followed by a melt curve analysis between 60 and 95 °C with a 0.5 °C increment every 5 seconds. The XPA forward primer fully targeted *XPA* exon 1, but all *XPA* reverse primers targeted over the respective exon junctions, annealing partially to each of the exons included in the junction. For expression normalization, the expression of the housekeeping gene *RPL13a* was included in the analysis. All primers used in this study are provided in Supplementary Table S4.

ETHICS STATEMENT

This study was conducted in accordance with protocols approved by the Research Ethics Committee of Guy's and St Thomas' Foundation Trust, London (reference 12/LO/0325, approved on April 17, 2018). Human primary cell lines included in this study were approved as part of this study protocol. All patients provided written informed consent to participate in the study and for the generation of primary fibroblast cell lines. Written permission was also obtained from the patients for publication of identifying images. This study was performed in accordance with the Declaration of Helsinki. The ethnicity of participants was identified by the medical team at the National Xeroderma Pigmentosum Service in London. These data were collected because disease prevalence, severity, and clinical outcomes vary significantly between populations, influencing the development of preventive strategies and tailored patient care.

DATA AVAILABILITY STATEMENT

No large datasets were generated, analyzed, or used during this study.

ORCID

Martijn Luijsterburg: http://orcid.org/0000-0001-5796-6541

CONFLICT OF INTEREST

The authors state no conflict of Interest

ACKNOWLEDGMENTS

We thank Areetha D'Souza (Vanderbilt University) for insightful discussions. We also thank Chi-Lin Tsai and John Tainer (MD Anderson) for providing purified TFIIH protein, Walter Chazin and Kaitlyn S. Gallagher (Vanderbilt University) for purified RPA protein, and Miaw-Sheue Tsai (Lawrence Berkeley National Laboratory) for help with expression of XPC-RAD23B, ERCC1-XPF, and XPG. We thank the patients and their families who are under the care of the National XP Clinic in the United Kingdom, funded by the National Health Service England Highly Specialized Services. This work was supported by the European Research Council Consolidator Grant STOP-FIX-GO (grant agreement number 101043815 to MSL) and the Netherlands Organisation for Scientific Research Vici grant (VI.C.212.005 to MSL). In addition, it was supported by grants from the Korean Institute for Basic Science (IBS-R022-A1 to ODS) and the National Cancer Institute (P01 CA092584 to ODS). MK was supported in part by the Basic Science Research Program through the National Research Foundation of Korea, funded by the Ministry of Education (RS-2023-00274772). The National XP Clinic in the United Kingdom is funded by the National Health Service England Highly Specialized Services.

AUTHOR CONTRIBUTIONS

Conceptualization: AvdH, HiF, ARL, ODS, MSL; Formal Analysis: AvdH, APW, MK, IB, HSK, HeF; Writing — Original Draft Preparation: AvdH, HiF, ARL, ODS, MSL

SUPPLEMENTARY MATERIAL

Supplementary material is linked to the online version of the paper at www.jidonline.org, and at https://doi.org/10.1016/j.jid.2025.08.047.

REFERENCES

Blee AM, Gallagher KS, Kim HS, Kim M, Kharat SS, Troll CR, et al. XPA tumor variant leads to defects in NER that sensitize cells to cisplatin. NAR Cancer 2024;6:zcae013.

Brosey CA, Chagot ME, Ehrhardt M, Pretto DI, Weiner BE, Chazin WJ. NMR analysis of the architecture and functional remodeling of a modular multidomain protein, RPA. J Am Chem Soc 2009;131:6346–7.

Calmels N, Botta E, Jia N, Fawcett H, Nardo T, Nakazawa Y, et al. Functional and clinical relevance of novel mutations in a large cohort of patients with Cockayne syndrome. J Med Genet 2018;55:329–43.

Cheon NY, Kim HS, Yeo JE, Schärer OD, Lee JY. Single-molecule visualization reveals the damage search mechanism for the human NER protein XPC-RAD23B. Nucleic Acids Res 2019;47:8337–47.

Cordts I, Önder D, Traschütz A, Kobeleva X, Karin I, Minnerop M, et al. Adult-onset neurodegeneration in nucleotide excision repair disorders (NERDND): time to move beyond the skin. Mov Disord 2022;37:1707–18.

Davis MW, Jorgensen EM. ApE, A plasmid editor: a freely available DNA manipulation and visualization program. Front Bioinform 2022;2:818619.

Enzlin JH, Schärer OD. The active site of the DNA repair endonuclease XPF-ERCC1 forms a highly conserved nuclease motif. EMBO J 2002;21:2045–53.

Evans E, Moggs JG, Hwang JR, Egly JM, Wood RD. Mechanism of open complex and dual incision formation by human nucleotide excision repair factors. EMBO J 1997;16:6559–73.

Fassihi H, Sethi M, Fawcett H, Wing J, Chandler N, Mohammed S, et al. Deep phenotyping of 89 xeroderma pigmentosum patients reveals unexpected heterogeneity dependent on the precise molecular defect. Proc Natl Acad Sci USA 2016;113:E1236–45.

Gradia SD, Ishida JP, Tsai MS, Jeans C, Tainer JA, Fuss JO. MacroBac: new technologies for robust and efficient large-scale production of recombinant multiprotein complexes. Methods Enzymol 2017;592:1–26.

Hohl M, Thorel F, Clarkson SG, Schärer OD. Structural determinants for substrate binding and catalysis by the structure-specific endonuclease XPG. J Biol Chem 2003;278:19500–8.

Itoh T. Xeroderma pigmentosum group E and DDB2, a smaller subunit of damage-specific DNA binding protein: proposed classification of xeroderma pigmentosum, Cockayne syndrome, and ultraviolet-sensitive syndrome. J Dermatol Sci 2006;41:87–96.

Khan SG, Metin A, Gozukara E, Inui H, Shahlavi T, Muniz-Medina V, et al. Two essential splice lariat branchpoint sequences in one intron in a xeroderma pigmentosum DNA repair gene: mutations result in reduced XPC mRNA levels that correlate with cancer risk. Hum Mol Genet 2004;13:343–52.

Khan SG, Yamanegi K, Zheng ZM, Boyle J, Imoto K, Oh KS, et al. XPC branch-point sequence mutations disrupt U2 snRNP binding, resulting in abnormal pre-mRNA splicing in xeroderma pigmentosum patients. Hum Mutat 2010;31:167–75.

Kim J, Li CL, Chen X, Cui Y, Golebiowski FM, Wang H, et al. Lesion recognition by XPC, TFIIH and XPA in DNA excision repair. Nature 2023;617:170–5.

Kim M, Kim HS, D'Souza A, Gallagher K, Jeong E, Topolska-Wós A, et al. Two interaction surfaces between XPA and RPA organize the preincision complex in nucleotide excision repair. Proc Natl Acad Sci USA 2022;119:e2207408119.

Kobayashi T, Takeuchi S, Saijo M, Nakatsu Y, Morioka H, Otsuka E, et al. Mutational analysis of a function of xeroderma pigmentosum group A (XPA) protein in strand-specific DNA repair. Nucleic Acids Res 1998;26:4662–8.

Kokic G, Chernev A, Tegunov D, Dienemann C, Urlaub H, Cramer P. Structural basis of TFIIH activation for nucleotide excision repair. Nat Commun 2019;10:2885.

Kraemer KH, Patronas NJ, Schiffmann R, Brooks BP, Tamura D, DiGiovanna JJ. Xeroderma pigmentosum, trichothiodystrophy and Cockayne syndrome: a complex genotype-phenotype relationship. Neuroscience 2007;145:1388–96.

Laugel V, Dalloz C, Durand M, Sauvanaud F, Kristensen U, Vincent MC, et al. Mutation update for the CSB/ERCC6 and CSA/ERCC8 genes involved in Cockayne syndrome. Hum Mutat 2010;31:113–26.

Lehmann AR. DNA repair-deficient diseases, xeroderma pigmentosum, Cockayne syndrome and trichothiodystrophy. Biochimie 2003;85:1101–11.

Luijsterburg MS, Goedhart J, Moser J, Kool H, Geverts B, Houtsmuller AB, et al. Dynamic in vivo interaction of DDB2 E3 ubiquitin ligase with UV-damaged DNA is independent of damage-recognition protein XPC. J Cell Sci 2007;120:2706–16.

Luijsterburg MS, Lindh M, Acs K, Vrouwe MG, Pines A, van Attikum H, et al. DDB2 promotes chromatin decondensation at UV-induced DNA damage. J Cell Biol 2012;197:267–81.

Mayne LV, Lehmann AR. Failure of RNA synthesis to recover after UV irradiation: an early defect in cells from individuals with Cockayne's syndrome and xeroderma pigmentosum. Cancer Res 1982;42:1473–8.

Missura M, Buterin T, Hindges R, Hübscher U, Kaspárková J, Brabec V, et al. Double-check probing of DNA bending and unwinding by XPA-RPA: an architectural function in DNA repair. EMBO J 2001;20:3554–64.

Moser J, Volker M, Kool H, Alekseev S, Vrieling H, Yasui A, et al. The UV-damaged DNA binding protein mediates efficient targeting of the nucleotide excision repair complex to UV-induced photo lesions. DNA Repair (Amst) 2005;4:571–82.

Nakazawa Y, Hara Y, Oka Y, Komine O, van den Heuvel D, Guo C, et al. Ubiquitination of DNA damage-stalled RNAPII promotes transcription-coupled repair. Cell 2020;180:1228–44.e24.

Nakazawa Y, Sasaki K, Mitsutake N, Matsuse M, Shimada M, Nardo T, et al. Mutations in UVSSA cause UV-sensitive syndrome and impair RNA polymerase IIo processing in transcription-coupled nucleotide-excision repair. Nat Genet 2012;44:586–92.

Nishigori C, Zghal M, Yagi T, Imamura S, Komoun MR, Takebe H. High prevalence of the point mutation in exon 6 of the xeroderma pigmentosum group A-complementing (XPAC) gene in xeroderma pigmentosum group A patients in Tunisia. Am J Hum Genet 1993;53:1001–6.

Postma M, Goedhart J. PlotsOfData-a web app for visualizing data together with their summaries. PLoS Biol 2019;17:e3000202.

Rapić-Otrin V, Navazza V, Nardo T, Botta E, McLenigan M, Bisi DC, et al. True XP group E patients have a defective UV-damaged DNA binding protein complex and mutations in DDB2 which reveal the functional domains of its p48 product. Hum Mol Genet 2003;12:1507–22.

Riedl T, Hanaoka F, Egly JM. The comings and goings of nucleotide excision repair factors on damaged DNA. EMBO J 2003;22:5293–303.

Sagun JP, Khan SG, Imoto K, Tamura D, Oh KS, DiGiovanna JJ, et al. Different germline variants in the XPA gene are associated with severe, intermediate,

or mild neurodegeneration in xeroderma pigmentosum patients. PLoS Genet 2024;20:e1011265.

Satokata I, Tanaka K, Miura N, Miyamoto I, Satoh Y, Kondo S, et al. Characterization of a splicing mutation in group A xeroderma pigmentosum. Proc Natl Acad Sci USA 1990;87:9908–12.

Satokata I, Tanaka K, Okada Y. Molecular basis of group A xeroderma pigmentosum: a missense mutation and two deletions located in a zinc finger consensus sequence of the XPAC gene. Hum Genet 1992a;88:603–7.

Satokata I, Tanaka K, Yuba S, Okada Y. Identification of splicing mutations of the last nucleotides of exons, a nonsense mutation, and a missense mutation of the XPAC gene as causes of group A xeroderma pigmentosum. Mutat Res 1992b;273:203–12.

Sethi M, Haque S, Fawcett H, Wing JF, Chandler N, Mohammed S, et al. A distinct genotype of XP complementation Group A: surprisingly mild phenotype highly prevalent in Northern India/Pakistan/Afghanistan. J Invest Dermatol 2016;136:869–72.

Sidwell RU, Sandison A, Wing J, Fawcett HD, Seet JE, Fisher C, et al. A novel mutation in the XPA gene associated with unusually mild clinical features in a patient who developed a spindle cell melanoma. Br J Dermatol 2006;155:81–8.

Sugasawa K, Hanaoka F. Sensing of DNA damage by XPC/Rad4: one protein for many lesions. Nat Struct Mol Biol 2007;14:887–8.

Sugasawa K, Ng JM, Masutani C, Iwai S, van der Spek PJ, Eker AP, et al. Xeroderma pigmentosum group C protein complex is the initiator of global genome nucleotide excision repair. Mol Cell 1998;2:223–32.

Sugitani N, Sivley RM, Perry KE, Capra JA, Chazin WJ. XPA: a key scaffold for human nucleotide excision repair. DNA Repair (Amst) 2016;44:123–35.

Takahashi Y, Endo Y, Sugiyama Y, Inoue S, Iijima M, Tomita Y, et al. XPA gene mutations resulting in subtle truncation of protein in xeroderma pigmentosum group A patients with mild skin symptoms. J Invest Dermatol 2010;130:2481–8.

Topolska-Woś AM, Sugitani N, Cordoba JJ, Le Meur KV, Le Meur RA, Kim HS, et al. A key interaction with RPA orients XPA in NER complexes. Nucleic Acids Res 2020;48:2173–88.

Typas D, Luijsterburg MS, Wiegant WW, Diakatou M, Helfricht A, Thijssen PE, et al. The de-ubiquitylating enzymes USP26 and USP37 regulate homologous recombination by counteracting RAP80. Nucleic Acids Res 2015;43:6919–33.

van den Heuvel D, Kim M, Wondergem AP, van der Meer PJ, Witkamp M, Lambregtse F, et al. A disease-associated XPA allele interferes with TFIIH binding and primarily affects transcription-coupled nucleotide excision repair. Proc Natl Acad Sci USA 2023;120:e2208860120.

van den Heuvel D, van der Weegen Y, Boer DEC, Ogi T, Luijsterburg MS. Transcription-coupled DNA repair: from mechanism to human disorder. Trends Cell Biol 2021;31:359–71.

van der Meer PJ, Van Den Heuvel D, Luijsterburg MS. Unscheduled DNA synthesis at sites of local UV-induced DNA damage to quantify global genome nucleotide excision repair activity in human cells. Bio Protoc 2023;13:e4609.

van der Weegen Y, de Lint K, van den Heuvel D, Nakazawa Y, Mevissen TET, van Schie JJM, et al. ELOF1 is a transcription-coupled DNA repair factor that directs RNA polymerase II ubiquitylation. Nat Cell Biol 2021;23:595–607.

van der Weegen Y, Golan-Berman H, Mevissen TET, Apelt K, González-Prieto R, Goedhart J, et al. The cooperative action of CSB, CSA, and UVSSA target TFIIH to DNA damage-stalled RNA polymerase II. Nat Commun 2020;11:2104.

Volker M, Moné MJ, Karmakar P, van Hoffen A, Schul W, Vermeulen W, et al. Sequential assembly of the nucleotide excision repair factors in vivo. Mol Cell 2001;8:213–24.

Weerd-Kastelein EA, Keijzer W, Sabour M, Parrington JM, Bootsma D. A xeroderma pigmentosum patient having a high residual activity of unscheduled DNA synthesis after UV is assigned to complementation group A. Mutat Res 1976;37:307–12.

SUPPLEMENTARY MATERIALS

SUPPLEMENTARY REFERENCES

Fassihi H, Sethi M, Fawcett H, Wing J, Chandler N, Mohammed S, et al. Deep phenotyping of 89 xeroderma pigmentosum patients reveals unexpected heterogeneity dependent on the precise molecular defect. Proc Natl Acad Sci USA 2016;113:E1236–45.

Kim J, Li CL, Chen X, Cui Y, Golebiowski FM, Wang H, et al. Lesion recognition by XPC, TFIIH and XPA in DNA excision repair. Nature 2023;617:170–5.

Typas D, Luijsterburg MS, Wiegant WW, Diakatou M, Helfricht A, Thijssen PE, et al. The de-ubiquitylating enzymes USP26 and USP37 regulate homologous recombination by counteracting RAP80. Nucleic Acids Res 2015;43:6919–33.

van den Heuvel D, Kim M, Wondergem AP, van der Meer PJ, Witkamp M, Lambregtse F, et al. A disease-associated XPA allele interferes with TFIIH binding and primarily affects transcription-coupled nucleotide excision repair. Proc Natl Acad Sci USA 2023;120:e2208860120.

van der Weegen Y, de Lint K, van den Heuvel D, Nakazawa Y, Mevissen TET, van Schie JJM, et al. ELOF1 is a transcription-coupled DNA repair factor that directs RNA polymerase II ubiquitylation. Nat Cell Biol 2021;23:595–607.

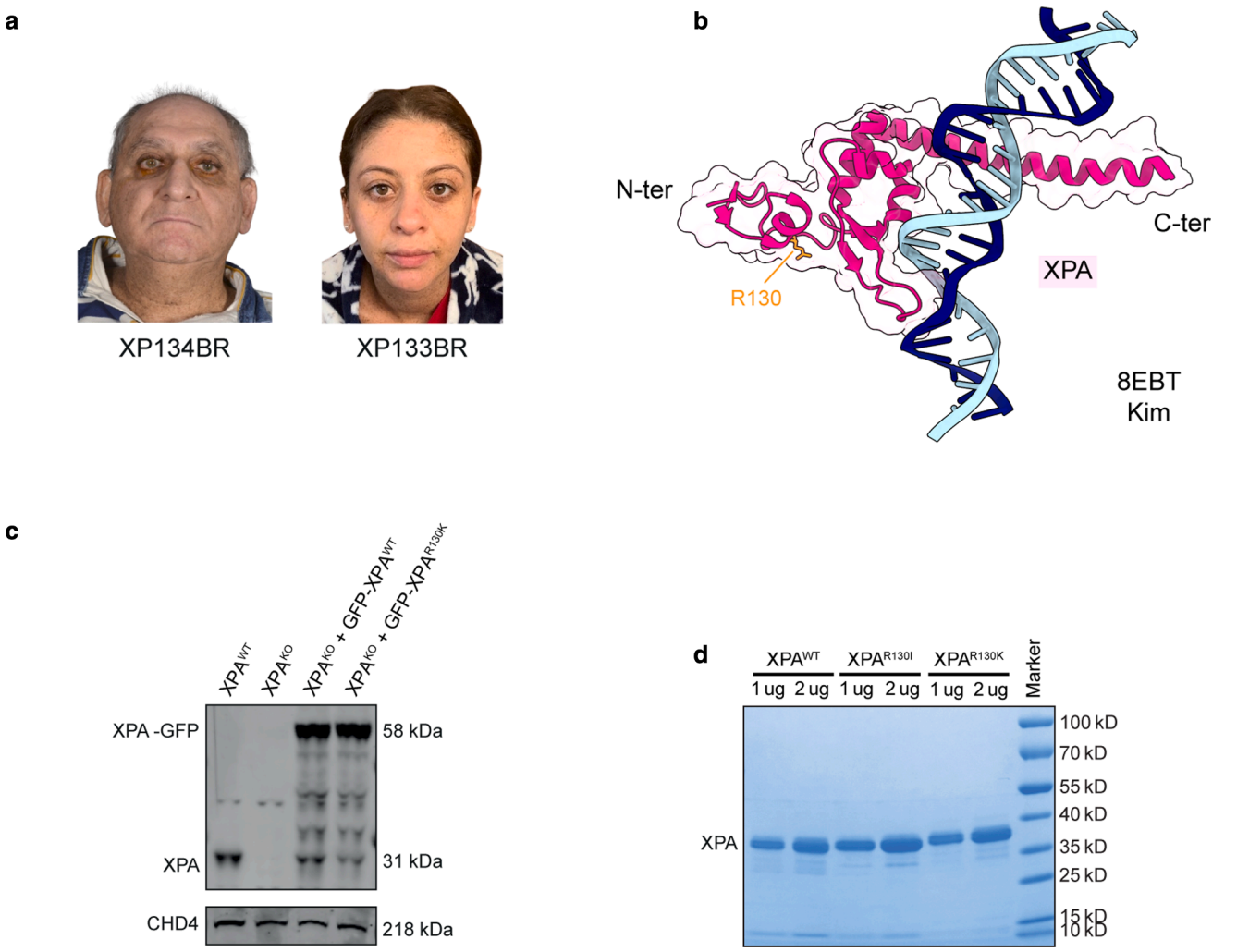

Supplementary Figure S1. Patient photographs and stability of XPA^{R130K}. (**a**) Picture of the XP-A patients XP134BR (left) and XP133BR (right). (**b**) Structure of XPA bound to DNA from a cryo-EM structure also containing XPC and TFIIH (8EBT [Kim et al, 2023]). The R130 residue is indicated. (**c**) Western blot of the indicated cell lines stained for XPA. The levels of CHD4 serve as loading control (**d**) Gel electrophoresis (Coomassie blue staining) of recombinant purified XPA variant proteins. Cryo-EM, cryogenic electron microscopy; XP, xeroderma pigmentosum.

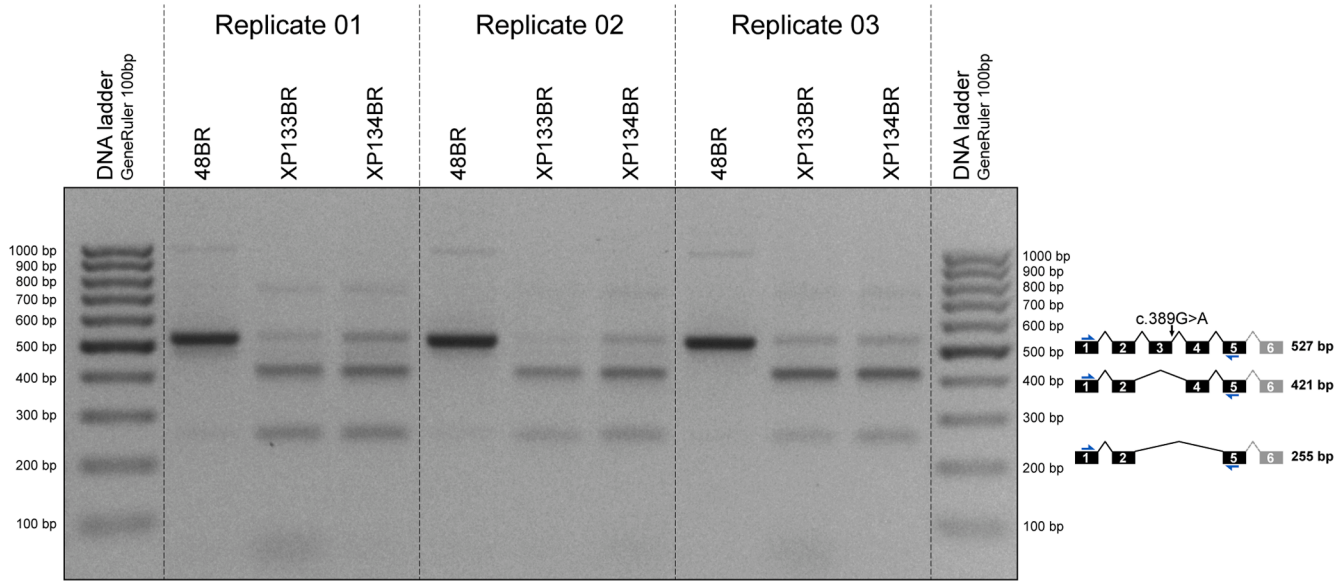

Supplementary Figure S2. Replicates of alternative XPA splicing analysis. Shown are 3 replicates of fragment length analysis (agarose gel electrophoresis) of the endpoint PCR of the *XPA* splice variants expressed in control (48BR) and patient-derived (XP133BR and XP134BR) primary fibroblasts. A schematic representation of each produced splice variant is depicted at each PCR product. The position of the c.389G>A variant and the location of the used primers (blue arrows) are indicated. Exon 6 is colored in gray because it was not included in this splicing analysis. XP, xeroderma pigmentosum.

Supplementary Table S1. Cell Lines

Cell Line	Genotype	Origin
48BR	Wild type	Alan Lehmann (University of Sussex, UK)
XP15BR	XPA: c.266_267dupAA; p.V90fs	Alan Lehmann (University of Sussex, UK) (Fassihi et al, 2016)
XP133BR	XPA: p.R130K	Alan Lehmann (University of Sussex, UK)
XP134BR	XPA: p.R130K	Alan Lehmann (University of Sussex, UK)
RPE1-hTERT-iCas9-PuroS-TP53-dKO (abbreviated to RPE WT)	RPE1-hTERT cells expressing inducible Cas9 (iCas9) and knockout for TP53 and PuroS (PAC)	van der Weegen et al (2021)
RPE XPA^{KO} (clone 01)	XPA knockout in RPE WT background	This study
RPE XPA^{KO} + GFP-XPA^{WT}	EGFP-XPA^{WT} rescue in RPE1 XPA-KO	This study
RPE XPA^{KO} + GFP-XPA^{R130K}	EGFP-XPA^{R130K} rescue in RPE1 XPA-KO	This study

Abbreviations: iCas9, inducible Cas9; KO, knockout; UK, United Kingdom; WT, wild type; XP, xeroderma pigmentosum.

Supplementary Table S2. Plasmids

Plasmids	Description	Origin	Identifier
pU6-sgXPA-PGK-puro-2A-tagBFP	Targets XPA exon 2: 5-GCCCCAAAGATAATTGACACAGG-3	Sigma-Aldrich library (van den Heuvel et al, 2023)	sgML#002, clone ID CR0054
pX458	Encodes Cas9	Addgene	pML#105
pEGFP-C1-IRES-PURO	Adjusted from pEGFP-C1 to insert IRES-Puro	(Typas et al, 2015)	pML#199
pPGK-EGFP-C1-IRES-PURO	Replaced the CMV promoter for a PGK promoter	(van der Weegen et al, 2021)	pML#244
pPGK-EGFP-XPA^{WT}-IRES-PURO	EGFP-XPA^{WT} coding sequence	(van den Heuvel et al, 2023)	pML#338
pPGK-EGFP-XPA^{R130K}-IRES-PURO	EGFP-XPA^{R130K} coding sequence	This study	pML#462

Abbreviations: ID, identification; WT, wild type; XP, xeroderma pigmentosum.

Supplementary Table S3. Antibodies

Antibody	Host	Origin	Dilution (Purpose) IF or WB	Identifier
XPA	Rabbit	Gift of R. Wood (CJ1)	1:10,000	aML #079
CHD4	Rabbit	Active Motif, 39289	1:1,000 (WB)	aML #019, RRID: AB_2614937
CPD	Mouse	Cosmo Bio, CAC-NM-DND-001	1:500 (IF)	aML #020, RRID:AB_1962813
Anti-mouse Alexa 555	Goat	Thermo Fisher Scientific, A-21424	1:1,000 (IF)	aML #015, RRID: AB_141780

Abbreviations: IF, Immunofluorescence; WB, western blot; XPA, xeroderma pigmentosum A.

Supplementary Table S4. Primers Used in XPA Splice Variant Analysis

Name	Identifier	Sequence
Primers used for XPA splice variant analysis by end-point PCR		
XPA-Exon1-Fw2	oML#1541	5′-CGAGTATCGAGCGGAAGC-3′
XPA-Exon5-Rv	oML#1513	5′-TTCTAATGCTTCTTGACTAC-3′
Primers used for quantitative XPA splice variant analysis (qPCR)		
XPA-Exon1-Fw3	oML#1661	5′-GCTGCGGCTACTGGAG-3′
XPA Ex2-3 splice-site_Rv	oML#1658	5′-TCCATAACAGGTCCTGGTTGA-3′ Exon2 overlapping sequence underlined
XPA Ex2-4 splice-site_Rv	oML#1659	5′-TTTATCATCAGCATCTCTGGTTGA-3′ Exon2 overlapping sequence underlined
XPA Ex2-5 splice-site_Rv	oML#1660	5′-GACCTCTTCACAATCTGGTTGA-3′ Exon2 overlapping sequence underlined
RPL13A_F	AH#23	5′-AACCTCCTCCTTTTCCAAGC-3′
RPL13A_R	AH#24	5′- GCAGTACCTGTTTAGCCACGA-3′

Abbreviations: Fw, forward; Rv, reverse; XPA, xeroderma pigmentosum A.